MULTIVARIATE SCALE-FREE DYNAMICS: TESTING FRACTAL CONNECTIVITY

S. Combrexelle[1], *H. Wendt*[1], *G. Didier*[2], *P. Abry*[3]

[1] IRIT-ENSEEIHT, CNRS (UMR 5505) , Université de Toulouse, France.
[2] Math. Dept., Tulane University, New Orleans, USA.
[3] Physics Dept., CNRS (UMR 5672), Ecole Normale Supérieure de Lyon, Université de Lyon, France.

ABSTRACT

Scale-free dynamics commonly appear in individual components of multivariate data. Yet, while the behavior of cross-components is crucial in modeling real-world multivariate data, their examination often suggests departures from exact multivariate self-similarity (also termed *fractal connectivity*). The present paper introduces a multivariate Gaussian stochastic process with Hadamard (i.e., entry-wise) self-similar scale-free dynamics, controlled by a matrix Hurst parameter H, that allows departures from fractal connectivity. The properties of its wavelet coefficients and wavelet spectrum are studied, enabling the estimation of H and of the fractal connectivity parameter. Furthermore, it permits the computation of closed-form confidence intervals for the estimates based on approximate (wavelet) covariances. Finally, these developments enable us to devise a test for fractal connectivity. Monte Carlo simulations are used to assess the accuracy of the proposed approximate confidence intervals and the performance of the fractal connectivity test.

***Index Terms*—** Multivariate self-similarity, Fractal connectivity, Wavelet spectrum, Hypothesis testing

1. INTRODUCTION

Context: univariate scale-free dynamics. The paradigm of scale-free dynamics has been ubiquitous in many real-world applications which are very different in nature, ranging from biomedical [1], to physics [2] to finance [3] and to Internet [4], to name but a few. Scale invariance implies that the dynamics of a time series $X(t)$ are driven by a wide continuum of time scales instead of only a few characteristic scales. Fractional Brownian motion (fBm), the only Gaussian self-similar process with stationary increments [5, 6], is among the most prominent and widely used scale invariance models for univariate time series. Its scale invariance properties are completely determined by a single parameter H, termed the Hurst or self-similarity parameter. The reference analysis tool is the wavelet transform. Given a univariate time series $X(t)$, it enables the estimation of H as the exponent controlling the power law behavior across scales a of the empirical second-order moments of its (ℓ_1-normalized, cf., (9)) wavelet coefficients $d_X(a,t)$ [7–9], i.e.,

$$\frac{1}{T}\sum_t d_X^2(a,t) \simeq Ca^{\alpha}, \quad \alpha = 2H, \tag{1}$$

where T is the number of terms in the sum.

Related works: multivariate scale-free dynamics. However, in many recent applications, data are collected by a large number m of sensors that jointly and simultaneously monitor one same system under study. *Multivariate* data, $X(t) = \big(X_q(t)\big)_{q=1}^m$, hence naturally call for multivariate scale-free dynamics models. To date, there has been a single reference model for multivariate scale-free dynamics, the so-called operator fractional Brownian motion (ofBm). The latter is a *multivariate self-similar* Gaussian process with stationary increments, and was recently been introduced in [10, 11]. In the present study, the focus is on a specific instance of ofBm, referred to as entry-wise scaling ofBm, denoted es-ofBm, in which each individual component $X_q(t)$ has scaling properties, as in (1) with scaling exponent $\alpha_{qq} = 2H_q$, $q = 1, \ldots, m$.

The estimation of the parameter vector $\big(H_q\big)_{q=1}^m$ has been theoretically studied in various settings [11, 12]. It can again be formulated in the wavelet domain, as in (1):

$$\frac{1}{T}\sum_t d^2_{X_q}(a,t) \simeq C_{qq}a^{\alpha_{qq}}, \tag{2}$$

Related works: fractal connectivity. By construction, es-ofBm further implies that, like auto-components, cross-components are also characterized by scale-free dynamics, which in wavelet representation translates into:

$$\frac{1}{T}\sum_t d_{X_i}(a,t)d_{X_l}(a,t) \simeq C_{il}a^{\alpha_{il}}. \tag{3}$$

However, the cross-scaling exponents α_{il} are, by definition, imposed by the auto-components, $\alpha_{il} = (\alpha_{ii} + \alpha_{qq})/2$, a property referred to as *fractal connectivity*, after [13, 14].

Although used in applications as a way of improving the estimation of the auto-component scaling exponents α_{qq} [13], fractal connectivity actually constitutes a severe practical limitation for the use of es-ofBm in the modeling of real-world data. Indeed, it restrictively implies that the only relevant information in the cross-term analysis of data is given by the correlation coefficient, a static property, hidden in the constant C_{il}. In other words, by contrast with the auto-terms, there is no relevant information conveyed by scale-free temporal dynamics of cross-terms.

There is however no reason to assume a priori that fractal connectivity holds in real-world data. To the contrary, there is a number of examples where scaling exponents empirically estimated on cross-terms significantly depart from the constraint $\alpha_{il} = (\alpha_{ii} + \alpha_{qq})/2$, and where such departures are actually regarded as crucial information (cf. e.g., [1] in neurosciences). In short, es-ofBm is too restrictive a model as it rules out the possibility that additional information on temporal dynamics may be obtained from the joint examination of pairs of components.

Goals, contributions and outline. Hence, there is a crucial need for practical procedures for testing departures from fractal connec-

Work supported by French ANR BLANC MULTIFRACS. G.D. was partially supported by the ARO grant W911NF-14-1-0475.

tivity (in the spirit of the preliminary attempt [14]) and for multivariate scale-free processes permitting to model such departures for real-world data. To address these limitations, the following original contributions are proposed. First, the Hadamard fractional Brownian motion (HfBm) is introduced, a multivariate process that enables pairwise departures from fractal connectivity (cf. Section 2). Second, the estimation of the auto- and cross-component scaling exponents of HfBm in a wavelet framework is defined and assessed (cf. Section 3). Third, an original procedure is devised that enables the approximate computation of the variances and covariances of the scaling exponent estimates from a single realization of a multivariate time series (cf. Section 4). Fourth, a practical test for fractal connectivity is devised, assessed and compared against a heuristic test proposed in [14] (cf. Section 5). The accuracy of the approximation and the performance of the proposed test are quantified by Monte Carlo simulations, conducted on synthetic copies of HfBm. Results indicate that the proposed theoretical developments are relevant and operational, and that the test for fractal connectivity significantly outperforms previous formulations.

2. HADAMARD SELF-SIMILAR PROCESS

Definition. Elaborating on univariate fBm [5, 6] and multivariate ofBm [10, 11], we propose to define Hadamard fractional Brownian motion (HfBm) $B_H = \{B_H(t)\}_{t\in\mathbb{R}} \in \mathbb{R}^m$ as a proper Gaussian process, with second moment given by:

$$\{\mathbb{E}[B_H(s)B_H(t)^*]\}_{s,t\in\mathbb{R}} = \left\{ \int_{\mathbb{R}} \left(\frac{e^{isx}-1}{ix}\right)\left(\frac{e^{-itx}-1}{-ix}\right) f_X(x)dx \right\}_{s,t\in\mathbb{R}}, \quad (4)$$

where the entries of the matrix of spectral densities f_X read:

$$f_X(x)_{il} = \left(\rho_{il}|x|^{-(\alpha_{il}-1)}\right) g_{il}(x), \quad i,l = 1,\dots,m \quad (5)$$

In (5), $\forall i,l = 1,\dots,m$, $0 < \alpha_{il} < 2$, $(\rho_{il})_{i,l=1}^m$ is a symmetric and positive definite point-covariance matrix, and the function g acts as a regularizing high-frequency (fine scale) cutoff that is necessary for the existence of HfBm. Indeed, the definition of multivariate spectral densities requires that [15]: $|f_{il}(x)| \le \sqrt{f_{ii}(x)}\sqrt{f_{ll}(x)}$ dx-a.e.. Preliminary analyses indicate that the simple choice $g_{ii}(x) \equiv 1$ and $g_{il}(x) \equiv \exp(-x^2)$ when $i \neq l$ guarantees the existence of the process in general, both with and without fractal connectivity [16].

Scale-free dynamics. HfBm is characterized by multivariate asymptotic (large-scale) scale-free dynamics in the sense that

$$(\mathbb{E}[B_H(as)B_H(at)^*])_{il} \simeq a^{2h_{il}} (\mathbb{E}[B_H(s)B_H(t)^*])_{il} \quad (6)$$

for $\forall a \gg 1$, with matrix exponent $H = (h_{il})_{i,l=1}^m$ satisfying

$$0 < h_{il} = \alpha_{il}/2 < 1, \quad i,l = 1,\dots,m. \quad (7)$$

Since the function g_{il} is a fine scale regularization, it does not impact coarse scale asymptotic scale-free dynamics. This intuition is confirmed by numerical simulations and will be formalized in [16].

Fractal connectivity. We also define the *fractal connectivity parameter* matrix, whose entries read:

$$\delta_{il} \triangleq (\alpha_{ii} + \alpha_{ll})/2 - \alpha_{il}, \quad 1 \le i \le l \le m. \quad (8)$$

The final aim of this work is to test whether $\delta_{il} = 0$, i.e., whether the components i and l are fractally connected, cf., Section 5. An HfBm with $\alpha_{il} = (\alpha_{ii} + \alpha_{ll})/2$ (i.e., satisfying fractal connectivity for all components), with $g_{il}(x) \equiv 1$ $\forall x, \forall (i,l)$ is an es-ofBm with parameters $(h_{11},\dots,h_{mm})$, as defined in [10, 11, 17].

3. SCALING EXPONENT WAVELET BASED ESTIMATION

Following seminal contributions on Hurst parameter estimation for univariate fBm [7, 18, 19] and bivariate ofBm [12], we make use of a wavelet framework for the estimation of the scaling parameters.

Discrete wavelet transform (DWT). A mother wavelet $\psi(t)$ is a (L^2 normalized) reference pattern with narrow time and frequency support that is furthermore characterized by its number of vanishing moments N_ψ, $\int_{\mathbb{R}} t^p\psi(t)dt = 0$ for $0 \le p < N_\psi$ and $\int_{\mathbb{R}} t^p\psi(t)dt \neq 0$ for $p \ge N_\psi$. Let $j \in \mathbb{N}$ and $k \in \mathbb{Z}$ denote the scale and a shift parameters, respectively. The vector-valued DWT coefficients of $X = \{X(t)\}_{t\in\mathbb{R}} \in \mathbb{R}^m$ are defined as [9]

$$D(j,k) = \left(d_q(j,k)\right)_{q=1}^m \triangleq \int_{\mathbb{R}} 2^{-j}\psi(2^{-j}t - k)X(t)dt. \quad (9)$$

Scale-free dynamics. Combining (6) and (9) permits translating HfBm scale-free dynamics into wavelet representations, $\forall\, j \gg 0$:

$$(\mathbb{E}[D(j,k)D(j,k)^*])_{il} \simeq C_{il}2^{j2h_{il}}\, \mathbb{E}[D(0,k)D(0,k)^*])_{il}. \quad (10)$$

Scaling exponent estimation procedure. The matrix $S(j)$ of empirical second-order moments of $D(j,k)$ reproduces the scaling relation in (10) for coarse scales $a = 2^j$, as

$$(S(j))_{il} \triangleq \left(\frac{1}{n_j}\sum_{k=1}^{n_j} D(j,k)D(j,k)^*\right)_{il} \simeq 2^{j2h_{il}}(S(0))_{il}. \quad (11)$$

Following classical univariate procedures, the scaling exponents $(\alpha_{il})_{i,l=1}^m$ can then be estimated by means of linear regressions:

$$\hat{\alpha}_{il} = \sum_{j=j_1}^{j_2} w_j \log_2 |S_{il}(j)|, \qquad 1 \le i \le l \le m, \quad (12)$$

where w_j is a suitable linear regression weight [7, 8, 11, 20, 21]. The resulting fractal connectivity parameter estimator is:

$$\hat{\delta}_{il} = (\hat{\alpha}_{ii} + \hat{\alpha}_{ll})/2 - \hat{\alpha}_{il}, \qquad i \neq l. \quad (13)$$

Estimation performance assessment. The estimation performance is assessed by means of Monte Carlo simulations, performed over 1000 independent realizations of bivariate ($m = 2$) HfBm for several (from small to large) sample sizes n, both under fractal connectivity ($\delta_{il} = 0$) and for departure from fractal connectivity ($\delta_{il} \neq 0$). HfBm synthesis is done by our own toolbox described in [22] and made available at hermir.org. It can be shown theoretically and validated numerically that estimates $\hat{\alpha}_{il}$ and $\hat{\delta}_{il}$ are asymptotically unbiased and have negligible finite sample size biases in practice. They are also asymptotically normal and their finite sample variances and covariances decrease as $1/n$. In essence, the performance replicates that achieved in the univariate setting, as well-documented and studied in, e.g., [19]. For space reasons, these theoretical results will be detailed in [16]. Instead, here we choose to put the emphasis on illustrating the asymptotic normality of the fractal connectivity parameter estimate $\hat{\delta}_{il}$, which is explicitly needed for the design of the fractal connectivity test in Section 5. Fig. 1 reports quantile-quantile plots of the empirical distribution of $\hat{\delta}_{il}$ against the standard Normal distribution. It shows that, while $\hat{\delta}_{il}$ can significantly depart from Gaussian for small sample size, it becomes practically indistinguishable from Gaussian for large sample size, both under fractal connectivity and under significant departures from that constraint.

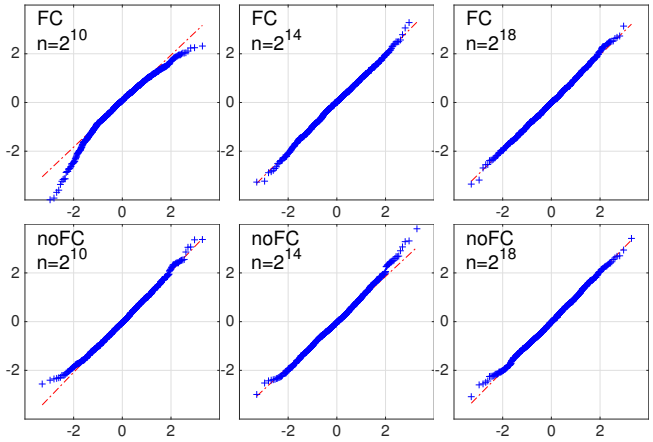

Fig. 1. Asymptotic normality of $\hat{\delta}_{il}$. Quantile plots of $\hat{\delta}_{12}$ for sample sizes $n = \{2^{10}, 2^{14}, 2^{18}\}$ (left to right column, respectively) for bivariate HfBm that are (top row) and are not (bottom row) fractally connected.

4. APPROXIMATE CLOSED-FORM EXPRESSIONS FOR THE COVARIANCES OF THE ESTIMATES

The next goal is to obtain reliable estimates of the covariances of the scaling and fractal connectivity parameters, which will allow applying the fractal connectivity test developed in Section 5.

Closed form analytical approximations for the (co)variances of $\hat{\alpha}_{il}$ and $\hat{\delta}_{il}$. To this end, approximate but closed-form analytical relations for these covariances are first obtained. The covariances of scaling exponent estimates are theoretically given by

$$\mathrm{Cov}[\hat{\alpha}_{is}, \hat{\alpha}_{lt}] = \sum_{j,j'=j_1}^{j_2} w_j w_{j'} \mathrm{Cov}[\log_2 S_{is}(j), \log_2 S_{lt}(j')]. \quad (14)$$

Relying on a Taylor expansion with Lagrange remainders for $f(X) = \log_2 |X|$, the following approximation can be computed:

$$\begin{aligned}\frac{\mathrm{Cov}[\hat{\alpha}_{is}, \hat{\alpha}_{lt}]}{(\log_2 \mathrm{e})^2} &\approx \sum_{j,j'=j_1}^{j_2} w_j w_{j'} \frac{\mathrm{Cov}[S_{is}(j), S_{lt}(j')]}{\mathbb{E}[S_{is}(j)]\mathbb{E}[S_{lt}(j')]} \\ &\approx \sum_{j,j'=j_1}^{j_2} w_j w_{j'} \left(\frac{\mathbb{E}[S_{is}(j) S_{lt}(j')]}{\mathbb{E}[S_{is}(j)]\mathbb{E}[S_{lt}(j')]} - 1 \right) \\ &\approx \sum_{j,j'=j_1}^{j_2} \frac{w_j w_{j'}}{n_j n_{j'}} \sum_{k=0}^{n_j-1} \sum_{k'=0}^{n_{j'}-1} \frac{\mathsf{r}_{il}(j,k;j',k') \mathsf{r}_{st}(j,k;j',k')}{\mathsf{r}_{is}(j,0;j,0)\mathsf{r}_{lt}(j',0;j',0)} \\ &\quad + \frac{\mathsf{r}_{it}(j,k;j',k')\mathsf{r}_{sl}(j,k;j',k')}{\mathsf{r}_{is}(j,0;j,0)\mathsf{r}_{lt}(j',0;j',0)}. \quad (15)\end{aligned}$$

In (15),

$$\begin{aligned}\mathsf{r}_{il}(j,k;j',k') &= \frac{\mathbb{E}[d_i(j,k) d_l(j',k')]}{\sqrt{\mathbb{E}[d_i^2(j,k)]\mathbb{E}[d_l^2(j',k')]}} \\ &= \mathsf{r}^0_{il} \frac{\Omega_{h_{il}}(j,k;j',k')}{\sqrt{\Omega_{h_{ii}}(j,k;j,k)\Omega_{h_{ll}}(j',k';j',k')}}, \quad (16)\end{aligned}$$

where $\mathsf{r}^0_{il} \triangleq \rho_{il}/\sqrt{\rho_{ii}\rho_{ll}}$ denotes the correlation coefficients amongst data components and $\Omega_{h_{il}}(j,k;j',k')$ the correlation amongst the wavelet coefficient of component i at scale 2^j and location $2^j k$, and that of component l at scale $2^{j'}$ and location $2^{j'}k'$.

$\sqrt{\mathrm{Var}_{\mathrm{approx}}/\mathrm{Var}_{\mathrm{MC}}}$	$\mathrm{Var}[\alpha_{11}]$	$\mathrm{Var}[\alpha_{12}]$	$\mathrm{Cov}[\alpha_{11}, \alpha_{22}]$	$\mathrm{Var}[\delta_{12}]$
$n = 2^{10}$	0.98	0.93	0.99	0.88
$n = 2^{12}$	0.97	0.92	0.92	0.87
$n = 2^{14}$	0.96	1.00	0.97	0.98
$n = 2^{16}$	0.98	1.00	1.05	0.97

Table 1. Estimation of $\mathrm{Var}[\boldsymbol{\alpha}_{(\cdot)}]$. Square roots of ratios of average of (co-)variances computed using (15) and (17) and of Monte Carlo (co-)variances (1000 independent realizations, $\mathsf{r}^0_{12} = 0.6$, $[\alpha_{11}, \alpha_{22}, \alpha_{12}] = [0.2, 0.6, 0.4]$).

The variances of the fractal connectivity parameters further read

$$\begin{aligned}\mathrm{Var}[\hat{\delta}_{il}] &= \mathrm{Var}[\hat{\alpha}_{il}] + (\mathrm{Var}[\hat{\alpha}_{ii}] + \mathrm{Var}[\hat{\alpha}_{ll}])/4 \\ &\quad + \mathrm{Cov}[\hat{\alpha}_{ii}, \hat{\alpha}_{ll}]/2 - \mathrm{Cov}[\hat{\alpha}_{ii}, \hat{\alpha}_{il}] - \mathrm{Cov}[\hat{\alpha}_{ll}, \hat{\alpha}_{il}]. \quad (17)\end{aligned}$$

Practical computation of $\boldsymbol{\Omega_{h_{il}}(j,k;j',k')}$. Let $h_j(k)$ and $g_j(k)$ denote the coefficients of the high and low pass filters associated to the practical iterative decomposition, at scale 2^j, of the DWT associated with the mother wavelet ψ [9]. Tedious but straightforward calculations show that $\Omega_{h_{il}}(j,k;j',k')$ can be made explicit as the convolution of the correlation of the process (cf. (6)) with that of the wavelets at scale 2^j:

$$\Omega_{h_{il}}(j,k;j',k') = ((g_j * \check{g}_{j'}) * \eta_{il})(k'-k), \quad \eta_{il}(\tau) = |\tau|^{\alpha_{il}} \quad (18)$$

where $\check{g}_j(k) \triangleq g_j(L-k)$, $k = 1, \ldots, L$.

Empirical estimates of the covariances of the estimates. In order to further enable the actual evaluation of (15) and (17) given a single realization of a multivariate time series X, the unknown parameters r^0_{il} and α_{il} in (18) are simply replaced by their estimates.

Assessment of the quality of the approximation. Monte Carlo simulations as described above are used to assess the overall quality of the estimates for the covariances of the estimates of the scaling exponents and variances for the estimates of the fractal connectivity parameters. Table 1 reports the assessment of the quality of such estimates in terms of the ratios of the (co)variance values obtained from the proposed approximations (15) and (17) to those obtained as averages over Monte Carlo estimates (1000 independent realizations). The results indicate that (15) and (17) yield reasonable (i.e., ratio close to 1) (co)variance estimates for small sample size ($n \leq 2^{12}$) and excellent estimates as the sample size increases ($n \geq 2^{14}$). This is a remarkable result, keeping in mind that the proposed estimates gather a number of assumptions: normality of the scaling exponent estimates, validity of the Taylor expansion, replacement of the theoretical values for r^0_{il} and α_{il} with their estimates.

It is also important to note that the absolute values in (12) were dropped for the analytical calculations detailed in the present section, which obviously only matters for cross-components. Intuitively, these absolute values play a minor role as soon as the correlations amongst data components become large. Conversely, when correlation between components is low, fractal connectivity parameters becomes irrelevant. It is thus a very satisfactory outcome that Monte Carlo simulations that incorporate these absolute values validate the proposed approximations that neglect them, both under fractal connectivity and under departures from that constraint. This issue, related to the validity of the Taylor expansion, will receive further theoretical investigations, that will be detailed in [16].

5. TESTING FRACTAL CONNECTIVITY

The analytical and empirical results of the previous sections are now used to address the final goal of the present work: practically testing fractal connectivity for a single finite length observation of data.

Test formulation. The null hypothesis of the test for a given pair of components reads:

$$H_0 : \ \delta_{il} = (\alpha_{ii} + \alpha_{ll})/2 - \alpha_{il} = 0, \qquad i \neq l.$$

Under H_0, assuming that $\mathsf{r}^0_{il} \neq 0$, the results of Section 3 lead us to conjecture that $\hat{\delta}_{il}$ is a zero mean Gaussian random variable asymptotically, i.e., $\hat{\delta}_{il} \overset{\mathrm{A}}{\sim} \mathcal{N}\left(0, \mathrm{Var}[\hat{\delta}_{il}]\right)$. Moreover, $\mathrm{Var}[\hat{\delta}_{il}]$ can be estimated by (15–17). A two-sided test with significance level s can thus be defined as

$$d_{\mathsf{s}} = \begin{cases} 1 & \text{if } \ |\hat{\delta}_{il}| > \mathrm{Var}[\hat{\delta}_{il}]^{1/2} \Phi^{-1}(1 - \mathsf{s}/2) \\ 0 & \text{otherwise,} \end{cases} \tag{19}$$

where $\Phi^{-1}(\cdot)$ is the inverse cumulative distribution function of the standard normal distribution.

Test performance assessment. We assess the performance of the test by applying it to 1000 independent realizations each of bivariate ($m = 2$) HfBm with exponents $[\alpha_{11}, \alpha_{22}] = [0.2, 0.6]$, $\delta_{12} = \{0;\ 0.05,\ 0.1,\ 0.15,\ 0.2\}$ and correlation level $\mathsf{r}^0_{12} = 0.7$ for sample sizes $n = \{2^{10}, 2^{12}, 2^{14}, 2^{16}\}$. A Daubechies wavelet with $N_\psi = 3$ vanishing moments is used, and scales for linear regressions are set to $j_1 = 2$ and j_2 the largest available scale. For each realization, the test decision (19) is evaluated using (17) with approximation (15). Estimates of the expected values of the test decisions, denoted by $\hat{d}_{\mathsf{s}}$, are then obtained as the averages over realizations of test decisions (19). The significance is set to $\mathsf{s} = 0.1$. The proposed test, denoted HFBM, is compared to the test described in [14], denoted WCF, which relies on the intuition that the wavelet coherence function of two components of a multivariate Gaussian scale invariant random process behaves approximately as

$$\Gamma_{il}(j) = S^{(il)}_{n_j}(j) / \sqrt{S^{(ii)}_{n_j}(j) S^{(ll)}_{n_j}(j)} \simeq \mathsf{r}^0_{il} 2^{j(\alpha_{12} - \frac{\alpha_{11}+\alpha_{22}}{2})}.$$

Instead of the rigorous statistical framework developed above, WCF is formulated using the observation that $\Gamma_{il}(j)$ corresponds to the Pearson Product-Moment correlation coefficient of $d_i(j, \cdot)$ and $d_l(j, \cdot)$. The Fisher's z statistics of $\Gamma_{il}(j)$ are hence approximately Gaussian, with known variances and, under H_0, with equal means across scales, and the test for H_0 is formulated as a test for the equality of means of Gaussian random variables, cf. [14] for details.

Performance under H_0. The results obtained under fractal connectivity, i.e., $(\alpha_{11} + \alpha_{22})/2 = \alpha_{12} = 0.4$, are reported in Table 2 (third row, $\delta_{12} = 0$) for the proposed test (top) and for the test in [14] (bottom). Note that under H_0, the average test decisions $\hat{d}_{\mathsf{s}}$ should equal the preset significance s. For the proposed test HFBM, the differences between $\hat{d}_{\mathsf{s}}$ and s are overall small, attaining only 4% for small sample size $n = 2^{10}$ and further decreasing with increasing sample size, as expected. This is consistent with the results reported in Table 1, where a small but systematic underestimation of $\mathrm{Var}[\hat{\delta}_{12}]$ for small sample sizes is observed. In contrast, the empirical significances $\hat{d}_{\mathsf{s}}$ of WCF are considerably larger than the preset value s, in particular for large sample sizes.

Test power. The power of the tests is assessed as the average test decisions under the alternative hypotheses $H_1 : \ \delta_{12} = \alpha_{12} - (\alpha_{11} + \alpha_{22})/2 \neq 0$ with $\delta_{12} = \{0.05,\ 0.1,\ 0.15,\ 0.2\}$. A direct comparison of the power of HFBM and WCF is, however, only meaningful for identical rejection probabilities under H_0. Since the performance of HFBM and WCF under H_0 differ, as discussed above, we adjust, for each sample size, the prescribed significance s to values $\tilde{\mathsf{s}}$ for which the average rejection rates under H_0 equal the target value, $\hat{d}_{\tilde{\mathsf{s}}} = 0.1$. The power of the tests is then estimated as the average test decisions $d_{\tilde{\mathsf{s}}}$ when H_1 is true. Results are reported in Table 2 (four columns on the right) and yield the following conclusions. First, the powers of both tests increase with sample size n and deviation from $\delta_{12} = 0$, as intuitively expected. Yet, HFBM is systematically and significantly more powerful than WCF and enables the detection a non-zero value for δ_{12} up to two times as often as WCF.

		$H_0 : \ \delta_{12} = 0$	$H_1 : \ \delta_{12} \neq 0$			
δ_{12}		0	0.05	0.1	0.15	0.2
HFBM	$n = 2^{10}$	14.0	25.4	43.5	66.1	84.5
	$n = 2^{12}$	10.9	63.6	96.8	99.8	100.0
	$n = 2^{14}$	11.2	99.2	100.0	100.0	100.0
	$n = 2^{16}$	10.9	100.0	100.0	100.0	100.0
WCF	$n = 2^{10}$	15.3	14.1	21.7	36.9	52.9
	$n = 2^{12}$	16.0	34.7	78.9	95.8	99.4
	$n = 2^{14}$	18.6	89.9	100.0	100.0	100.0
	$n = 2^{16}$	22.5	100.0	100.0	100.0	100.0

Table 2. **Test performance.** Average (over 1000 realizations) test decisions $\hat{d}_{\mathsf{s}}$ (in %) obtained with HFBM and WCF for different sample sizes n. Left column: under $H_0 : \ \delta_{12} = 0$, with preset significance $\mathsf{s} = 10\%$. Right columns: under $H_1 : \ \delta_{12} \neq 0$, $\delta_{12} = \{0.05,\ 0.1,\ 0.15,\ 0.2\}$, with significance s adjusted such that the rejection rate would equal 10% under H_0.

Overall, these results confirm that the proposed developments are operational and can be relevantly applied in the investigation of scale-free dynamics and testing of fractal connectivity in multivariate time series.

6. CONCLUSIONS

In this contribution, a flexible and versatile multivariate self-similar process has been introduced, the Hadamard fractional Brownian (HfBm) motion. It enables the relevant modeling of the joint scale-free dynamics of multivariate time series, allowing situations where cross-components are not fractally connected. The analysis of the auto and cross-component scaling exponents was conducted by means of a wavelet-based estimation procedure. Moreover, an original procedure for obtaining estimates of the variances and covariances of the scaling exponents was also devised and studied. Finally, based on these developments, a test for fractal connectivity of pairs of time series components was put forward. Monte Carlo simulations, relying on synthetic copies of HfBm, using a procedure designed by ourselves, confirm the relevance of the proposed developments and indicate the superior performance of the fractal connectivity test as compared to previous formulations. Future work will include further theoretical studies of HfBm properties, as well as of formal issues in the derivation of the approximations proposed here. These will be reported in [16]. Estimation and test procedures will also be used in several applications, notably in neurosciences, elaborating on work completed in [23] .

7. REFERENCES

[1] P. Ciuciu, P. Abry, and B. J. He, "Interplay between functional connectivity and scale-free dynamics in intrinsic fMRI networks," *Neuroimage*, vol. 95, pp. 248–263, 2014.

[2] B.B. Mandelbrot, "Intermittent turbulence in self-similar cascades: divergence of high moments and dimension of the carrier," *J. Fluid Mech.*, vol. 62, pp. 331–358, 1974.

[3] B.B. Mandelbrot, "A multifractal walk down Wall Street," *Sci. Am.*, vol. 280, no. 2, pp. 70–73, 1999.

[4] P. Abry, R. Baraniuk, P. Flandrin, R. Riedi, and D. Veitch, "Multiscale nature of network traffic," *IEEE Signal Proces. Mag.*, vol. 19, no. 3, pp. 28–46, May 2002.

[5] B.B. Mandelbrot and J.W. van Ness, "Fractional Brownian motion, fractional noises and applications," *SIAM Reviews*, vol. 10, pp. 422–437, 1968.

[6] G. Samorodnitsky and M. Taqqu, *Stable non-Gaussian random processes*, Chapman and Hall, New York, 1994.

[7] P. Flandrin, "Wavelet analysis and synthesis of fractional Brownian motion," *IEEE Trans. Info. Theory*, vol. 38, no. 2, pp. 910–917, 1992.

[8] D. Veitch and P. Abry, "A wavelet-based joint estimator of the parameters of long-range dependence," *IEEE Trans. Info. Theory*, vol. 45, no. 3, pp. 878–897, 1999.

[9] S. Mallat, *A Wavelet Tour of Signal Processing*, Academic Press, San Diego, CA, 1998.

[10] G. Didier and V. Pipiras, "Integral representations and properties of operator fractional Brownian motions," *Bernoulli*, vol. 17, no. 1, pp. 1–33, 2011.

[11] P.-O. Amblard and J.-F. Coeurjolly, "Identification of the multivariate fractional Brownian motion," *IEEE Trans. Signal Proces.*, vol. 59, no. 11, pp. 5152–5168, 2011.

[12] P. Abry and G. Didier, "Wavelet estimation for operator fractional Brownian motion," *Bernoulli*, 2016, to appear.

[13] S. Achard, D. S. Bassett, A. Meyer-Lindenberg, and E. Bullmore, "Fractal connectivity of long-memory networks," *Phys. Rev. E*, vol. 77, no. 3, pp. 036104, 2008.

[14] H. Wendt, A. Scherrer, P. Abry, and S. Achard, "Testing fractal connectivity in multivariate long memory processes," in *Proc. IEEE Int. Conf. Acoust., Speech, and Signal Proces. (ICASSP)*, Taipei, Taiwan, 2009, pp. 2913–2916.

[15] P. J. Brockwell and R. A. Davis, *Time series: theory and methods*, Springer Science & Business Media, 1991.

[16] H. Wendt, G. Didier, S. Combrexelle, and P. Abry, "Multivariate Hadamard self-similarity: testing fractal connectivity," *in preparation*, 2017.

[17] J.-F. Coeurjolly, P.-O. Amblard, and S. Achard, "Wavelet analysis of the multivariate fractional Brownian motion," *ESAIM: Probability and Statistics*, vol. 17, pp. 592–604, 2013.

[18] P. Abry and D. Veitch, "Wavelet analysis of long-range dependent traffic.," *IEEE Trans. on Info. Theory*, vol. 44, no. 1, pp. 2–15, 1998.

[19] D. Veitch and P. Abry, "A wavelet-based joint estimator of the parameters of long-range dependence," *IEEE Trans. Info. Theory*, vol. 45, no. 3, pp. 878–897, 1999.

[20] P. Abry, P. Flandrin, M. Taqqu, and D. Veitch, "Wavelets for the analysis, estimation and synthesis of scaling data," in *Self-similar Network Traffic and Performance Evaluation*. spring 2000, Wiley.

[21] H. Wendt, P. Abry, and S. Jaffard, "Bootstrap for empirical multifractal analysis," *IEEE Signal Proces. Mag.*, vol. 24, no. 4, pp. 38–48, 2007.

[22] H. Helgason, V. Pipiras, and P. Abry, "Synthesis of multivariate stationary series with prescribed marginal distributions and covariance using circulant matrix embedding," *Signal Proces.*, vol. 91, no. 8, pp. 1741 – 1758, 2011.

[23] P. Ciuciu, P. Abry, and B. J. He, "Interplay between functional connectivity and scale-free dynamics in intrinsic fmri networks," *NeuroImage*, vol. 95, no. 186, pp. 248–263, 2014.